nature physics

Article

https://doi.org/10.1038/s41567-023-02366-z

Time reversibility during the ageing of materials

Received: 24 April 2023

Accepted: 30 November 2023

Published online: 26 January 2024

Check for updates

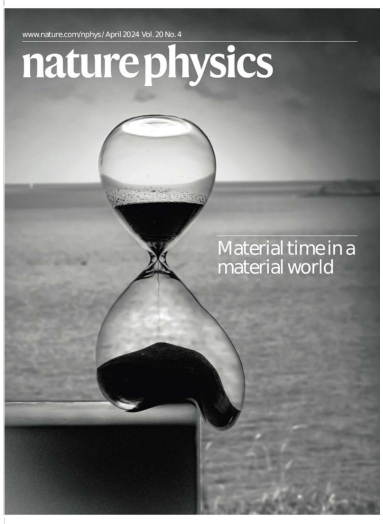

Till Böhmer[1], Jan P. Gabriel[2], Lorenzo Costigliola[2], Jan-Niklas Kociok[1], Tina Hecksher[2], Jeppe C. Dyre[2] & Thomas Blochowicz[1]

Physical ageing is the generic term for irreversible processes in glassy materials resulting from molecular rearrangements. One formalism for describing such ageing processes involves the concept of material time, which may be thought of as time measured on a clock whose rate changes as the glass ages. Experimental determination of material time has so far not been realized, however. Here we show how dynamic light-scattering measurements provide a way forward. We determined the material time for an ageing sample of the glass-former 1-phenyl-1-propanol after temperature jumps close to the glass transition from the time-autocorrelation function of the intensity fluctuations probed by multispeckle dynamic light scattering. These fluctuations are shown to be stationary and reversible when regarded as a function of the material time. The glass-forming colloidal synthetic clay Laponite and a chemically ageing curing epoxy are also shown to display material-time-reversible scattered-light intensity fluctuations, and simulations of an ageing binary system monitoring the potential energy confirm material-time reversibility. In addition to demonstrating direct measurements of the material time, our findings identify a fundamental property of ageing in quite different contexts that presents a challenge to the current theories of ageing.

Few persons would claim that time can be reversed—all living creatures age and eventually die, a dropped glass breaks while the reverse never happens, mixing cold and warm water leads irreversibly to an intermediate temperature and so on[1]. On the other hand, the fundamental equation-of-motion laws of nature are all time reversible: for example, Newton's laws of classical mechanics, the Schrödinger equation of quantum mechanics, Maxwell's equations for electromagnetism and the Einstein equation of gravity and spacetime. The irreversibility of everyday life is accounted for by the second law of thermodynamics, which states that the entropy of an isolated system can increase or stay constant but never decrease[2,3].

When entropy is constant in time, the system in question is in thermal equilibrium. Reflecting the time reversibility of the fundamental laws, thermal-equilibrium fluctuations are statistically time reversible. As shown by Onsager in 1931, this reversibility leads to quantitative relations between coefficients describing small, linear deviations from equilibrium[4]. This paper presents ageing data that go far beyond the linear-response regime, but are nevertheless shown to be statistically reversible when regarded as functions of the so-called material time that controls ageing according to the classical Tool–Narayanaswamy (TN) formalism[5,6]. This goes against the conventional wisdom according to which ageing is fundamentally irreversible, involving plasticity, dissipation, entropy production and dynamical heterogeneities with a correlation length that changes during ageing. Our findings from light-scattering experiments on three quite different samples, confirmed by computer simulations of a simple model system, bring into question the status of ageing as a prototypical case of non-equilibrium thermodynamics[7].

[1]Institute for Condensed Matter Physics, Technical University of Darmstadt, Darmstadt, Germany. [2]Glass and Time, IMFUFA, Department of Science and Environment, Roskilde University, Roskilde, Denmark. e-mail: till.boehmer@pkm.tu-darmstadt.de; dyre@ruc.dk; thomas.blochowicz@physik.tu-darmstadt.de

https://doi.org/10.1038/s41567-023-02366-z

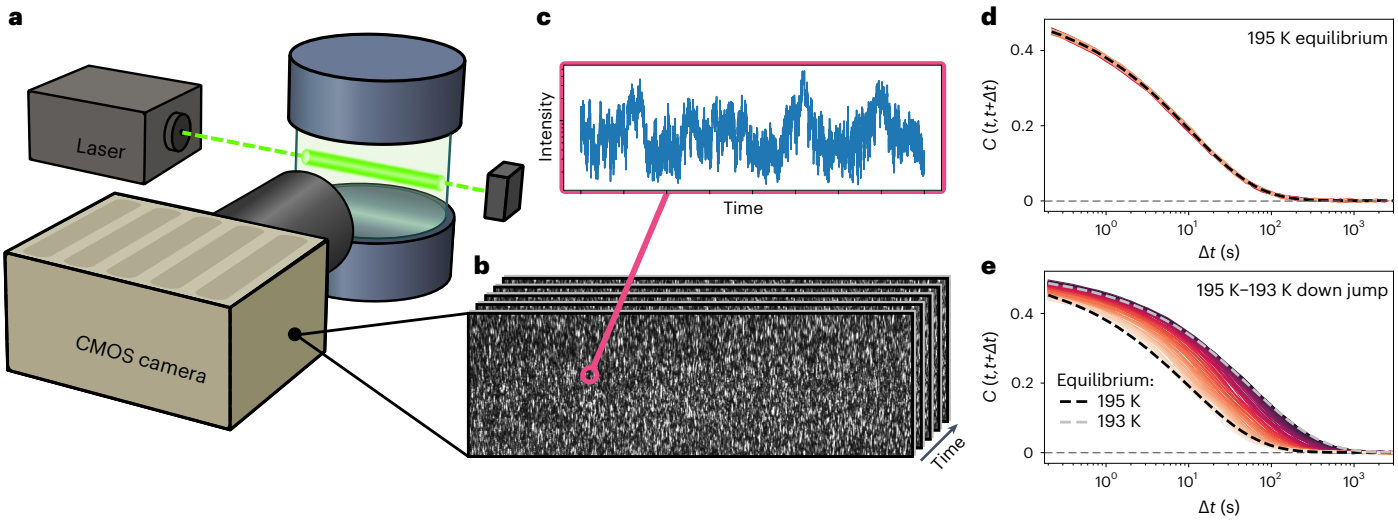

Fig. 1 | Multispeckle DLS. a,**b**, The sample is illuminated by a laser beam (**a**), and an sCMOS camera is used to detect the speckle pattern (**b**) of the 90° scattered-light intensity. **c**, In each speckle statistically independent temporal intensity fluctuations are observed. The time-autocorrelation function $C(t, t + \Delta t)$ is obtained as the multispeckle average. **d**, Data for 1P1P in thermal equilibrium at 195 K where $C(t, t + \Delta t)$ is stationary, that is, depends only on Δt. **e**, During physical ageing following a temperature down jump, $C(t, t + \Delta t)$ changes with t for fixed Δt. The evolution starts from the equilibrium time-autocorrelation function at the initial temperature 195 K (left dashed curve) and ends in equilibrium at the annealing temperature 193 K (right dashed curve). The different colours correspond to different t evenly spaced on a logarithmic axis.

Physical ageing

In contrast to degradation involving chemical reactions as in corrosion, physical ageing involves changes of material properties that are caused exclusively by molecular rearrangements[8–16]. Non-crystalline materials such as ordinary glass[6,9], polymers[10,13,17] and metallic glasses[14,18,19] are all subject to physical ageing because the glassy state relaxes continuously towards a state of metastable equilibrium[20]. In the vast majority of cases this is too slow to be observed, but in certain cases physical ageing results in undesirable property changes. The study of physical ageing is important for applications of glassy materials, as well as for optimization of their production. For this reason—and because what controls the rate of physical ageing remains disputed—this old research field continues to attract attention[21–27].

The best controlled physical ageing experiments involve a rapid change of temperature starting from a state of (metastable) thermal equilibrium, after which the system's path towards equilibrium at a fixed 'annealing' temperature is monitored by continuously measuring some physical property. The outcome of such a temperature-jump experiment depends critically on whether a jump up or down is considered. Comparing up and down jumps to the same temperature, the latter are substantially faster and more stretched in time than up jumps[9,13]. Even jumps involving just a 1% temperature change result in quite different relaxations towards equilibrium, in some cases with more than a decade difference in average relaxation time. This 'asymmetry of approach' implies that physical ageing is highly nonlinear[9,13,28].

In many experiments physical ageing is well described in terms of the so-called material time[9]. This concept was introduced in 1971 by Narayanaswamy, who, as an engineer at Ford Motor Co., sought the cooling protocol for generating optimal frozen-in stresses in the production of windscreens[6]. The material time may be thought of as time measured on a clock whose rate changes as the glass ages. Conceptually, this is analogous to the proper-time concept of the theory of relativity, the time measured on a clock following a moving observer. The material-time approach to physical ageing is termed the TN formalism[9,13], an equivalent of which was developed a few years later for ageing polymers[29]. The striking mathematical simplification of TN is that physical ageing becomes linear when described in terms of the material time. Thus, for all temperature jumps, a given quantity relaxes towards equilibrium following the same function of the material time, except for an amplitude scaling in proportion to the jump magnitude.

Specifically, when the temperature history is parameterized in terms of material time ξ, the TN formalism describes ageing by a linear convolution integral over the temperature-variation history[6,9,17]. Using instead the laboratory time as parameter, the linear limit is only approached for temperature variations in the millikelvin range. The fundamental prediction of TN is that knowledge of this linear limit is enough to determine the highly nonlinear ageing phenomenon. This was recently verified reporting temperature jumps of amplitude down to 10 mK (ref. 30).

According to the TN formalism, linear-response theory applies for the material-time development of average quantities. By the fluctuation–dissipation theorem[3], a linear response reflects equilibrium thermal fluctuations that are time reversible, which suggests that fluctuations monitored during ageing are reversible if regarded as a function of the material time instead of the laboratory time. Here 'reversible' means that past and future cannot be distinguished in the statistical properties. This conjecture is investigated in this Article. To do so it is necessary to both measure thermal fluctuations and determine the material time during the ageing.

Our main experimental technique is dynamic light scattering (DLS)[31]. Compared with other experimental methods used for probing ageing dynamics (for example, dielectric spectroscopy), the DLS set-up operates in the time domain. With few exceptions[32], frequency-domain experiments average over several sinusoidal cycles, during which the ageing material may change properties. In contrast, time-domain experiments can, at least in principle, access 'instantaneous' autocorrelation or response functions that are well defined even if ageing and correlation decay take place on comparable timescales. To determine the material time as a function of the time t, $\xi(t)$, we assume in the TN spirit that the normalized scattered-light intensity time-autocorrelation function as a function of t_1 and t_2 is determined by the material-time difference $\xi(t_2) - \xi(t_1)$. As shown below, this leads to predictions that were discussed for spin-glasses in a seminal paper by Cugliandolo and Kurchan from 1994[33]—a paper, however, that did not discuss how an ageing system approaches thermal equilibrium.

https://doi.org/10.1038/s41567-023-02366-z

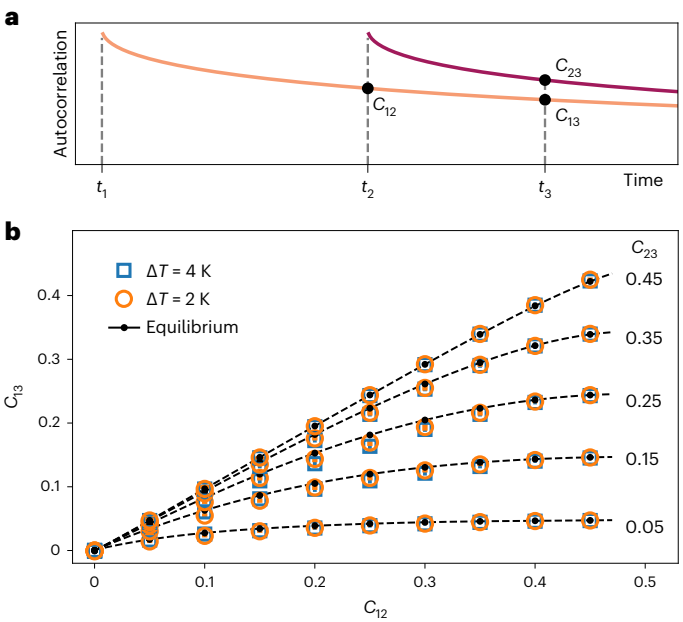

Fig. 2 | Verifying the triangular relation. a, Schematic illustration of how C_{12}, C_{13} and C_{23} are defined for $t_1 < t_2 < t_3$. **b**, Average C_{13} plotted versus C_{12} for fixed values of C_{23} (1P1P data). The data refer to thermal equilibrium at 193 K, as well as to physical ageing following two different temperature down jumps to 193 K. The relation between the three time-autocorrelation functions of the two temperature jumps is the same as in equilibrium. The s.d. of the C_{13} data (for a total of $n = 2.8561 \times 10^7$ triangles) are given as error bars (smaller than the symbol size, <0.01). These data confirm the triangular relation equation (2), which expresses a necessary requirement for using the intensity time-autocorrelation function to define the material time.

It is an experimental challenge to obtain reliable thermal-fluctuation time-autocorrelation data during ageing because one cannot use the standard procedure of ensemble averaging by a moving time average. We determine the ensemble average for an ageing sample by simultaneously measuring several time-autocorrelation functions with a camera monitoring thousands of so-called speckles, that is, the granular interference pattern of the scattered light (Fig. 1b). From these data we extract the material time. Using standard methods of time-series analysis it is then demonstrated that, when regarded as a function of the material time, the fluctuations are stationary and reversible. These findings for the molecular system 1-phenyl-1-propanol (1P1P) apply also for the colloidal synthetic clay Laponite studied by VV (polarized) light scattering, which, in contrast to the molecular system, does not approach equilibrium within the time of observation. In search of a counterexample we also studied a curing epoxy that ages chemically by continuous polymerization. However, this system also exhibits material-time reversal invariance; apparently, this property is not limited to physically ageing systems. Finally, material-time reversibility is shown to apply also for the potential-energy fluctuations of an ageing computer-simulated model liquid.

Experimental methods in brief

We use depolarized DLS to probe the temporal intensity fluctuations of light scattered at 90° from the ageing sample. These fluctuations reflect the rotational dynamics of the molecules on the molecular scale (see Supplementary Information for details), which is quantified by the intensity time-autocorrelation function. In standard equilibrium DLS experiments the latter is determined via a moving time average of the product of two intensities separated by a fixed time interval Δt, but as mentioned this cannot be done for an ageing sample. To obtain acceptable statistics we perform a multispeckle DLS experiment that probes a large speckle pattern using an sCMOS (scientific complementary metal–oxide–semiconductor) camera with ten pictures taken per second; compare Fig. 1a,b. The intensity fluctuations of different speckles (Fig. 1c) are statistically independent, so the time-resolved ensemble-averaged intensity time-autocorrelation function $\langle I(t)I(t+\Delta t)\rangle$ can be determined, in which the angular brackets are averages over the different speckles. This is the main idea; more details are given in Methods.

Time-resolved multispeckle light scattering has been applied to monitor ageing and ultraslow dynamics of colloidal glasses, gels and foams, mainly in the diffusing-wave regime[34–38], but so far this technique has not been used to monitor non-equilibrium molecular systems. The procedure of calculating multipixel averages to obtain time-resolved autocorrelations has also been used in connection with X-ray photon correlation spectroscopy, for example, for studying the physical ageing of metallic glasses[39–41].

If the intensity of the scattered light at time t at one pixel is denoted by $I(t)$, the normalized intensity time-autocorrelation function is defined by $C(t_1, t_2) \equiv \langle I(t_1)I(t_2)\rangle / [\langle I(t_1)\rangle\langle I(t_2)\rangle] - 1$. The normalized intensity time-autocorrelation function $C(t, t+\Delta t)$ of supercooled 1P1P in equilibrium is plotted in Fig. 1d as a function of Δt for different times t (different colours). The data collapse onto a single curve, confirming stationarity of the equilibrium state. In contrast, a distinct t dependence of $C(t, t+\Delta t)$ is observed following a temperature down jump as shown in Fig. 1e, where darker colours correspond to larger t. Starting from the initial equilibrium state at 195 K (left dashed curve), the rate of decay of $C(t, t+\Delta t)$ to zero as $\Delta t \to \infty$ slows down with increasing t. Eventually a new stationary equilibrium state is approached at the annealing temperature, 193 K (right dashed curve).

Identifying the material time

We determine ξ as a function of time from the assumption that $C(t_1, t_2)$ reflects the elapsed material time between t_1 and t_2. Thus, it is assumed[42] that for some monotonic function that goes to zero for $x \to \infty$, $F(x)$, one has

$$C(t_1, t_2) = F(\xi(t_2) - \xi(t_1)) . \tag{1}$$

For this to apply for any t_1 and t_2, the following consistency requirement must be obeyed. Since $\xi(t_3) - \xi(t_1) = \xi(t_2) - \xi(t_1) + \xi(t_3) - \xi(t_2)$, $C(t_1, t_3)$ is determined by $C(t_1, t_2)$ and $C(t_2, t_3)$ (ref. 43). This property always applies in thermal equilibrium because in that case $C(t_1, t_2)$ is a function of $t_2 - t_1$, which is proportional to $\xi(t_2) - \xi(t_1)$ since ξ in equilibrium is a linear function of t. During ageing, however, the consistency requirement is non-trivial, as ξ is no longer a linear function of t because the structure changes with time.

Introducing the abbreviated notation $C_{12} = C(t_1, t_2)$ and so on, the above translates into the so-called triangular relation that was originally derived by Cugliandolo and Kurchan in 1994 in a mean-field calculation of time-autocorrelation functions of infinite-range spin systems quenched from infinite to a low temperature[33],

$$C_{13} = C_{13}(C_{12}, C_{23}) . \tag{2}$$

This equation expresses that, for any t_2, C_{12} and C_{23} determine C_{13}. Equilibrium dynamics is time reversible, which implies symmetry of the function C_{13},

$$C_{13}(C_{12}, C_{23}) = C_{13}(C_{23}, C_{12}) . \tag{3}$$

This symmetry is inherited from equilibrium for an ageing sample, a result that was derived by a different argument in ref. 33.

We checked equation (2) by calculating C_{12}, C_{23} and C_{13} for several million time triplets, $t_1 < t_2 < t_3$, as illustrated in Fig. 2a. By binning

https://doi.org/10.1038/s41567-023-02366-z

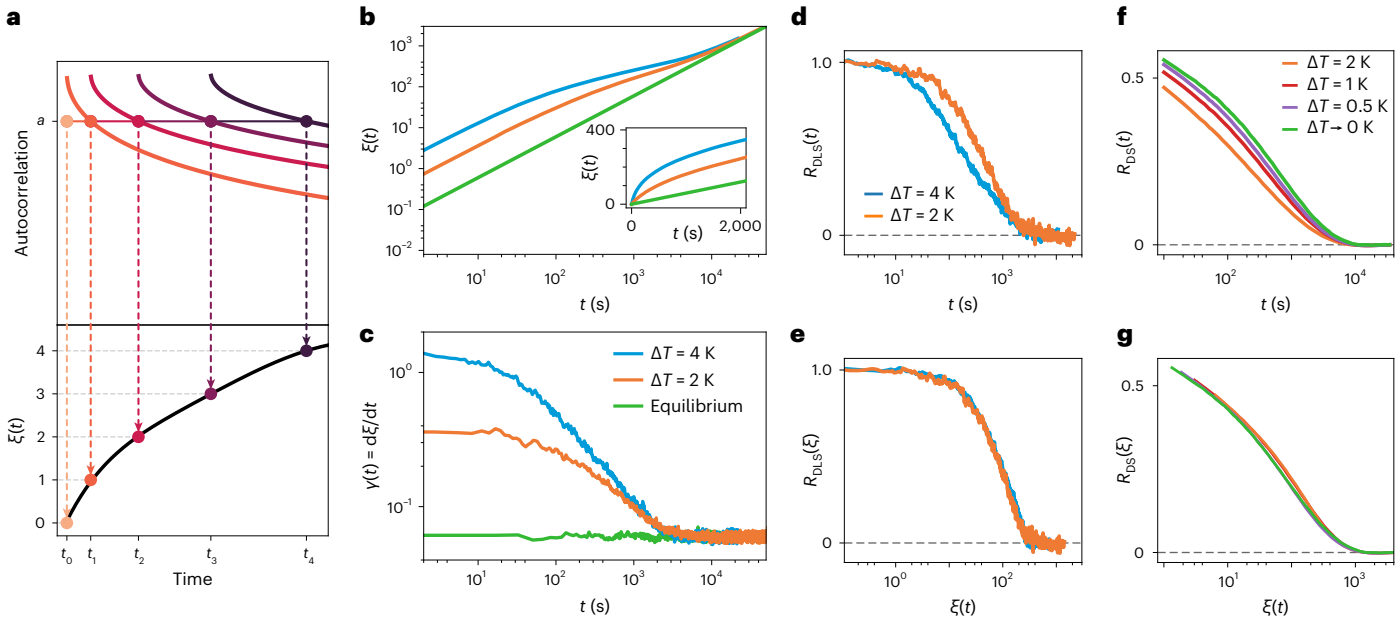

Fig. 3 | Determining and validating the material time for down jumps to 193 K. a, Schematic illustration of how ξ is identified step by step as a function of the laboratory time t. The time-autocorrelation functions are plotted here on a linear time scale, in contrast to the logarithmic time scale used in Fig. 1. **b**, $\xi(t)$ in a logarithmic representation for different temperature jumps and in thermal equilibrium (the colours are defined in **c**). At short times the samples have aged negligibly and $\xi(t)$ is a linear function of time; the same linear time dependence applies in equilibrium that is approached for $t \to \infty$. The inset shows the same data in a linear representation (the 4 K data were adapted to compensate for a slightly different annealing temperature; Supplementary Information). **c**, The ageing rate γ (equation (5)) as a function of t. Initially, γ is large because the 'material-time clock' ticks fast; as the ageing proceeds γ approaches its equilibrium value. **d**, When considered as a function of the laboratory time, due to the fact that ageing is nonlinear, the normalized relaxation functions (equation (6)) differ in shape for the two temperature jumps. **e**, The transformation $t \to \xi(t)$ collapses the normalized relaxation functions. **f**, Nonlinearity of physical ageing is evident also for the dielectric loss relaxation function $R_{DS}(t)$. The green curve gives data for a temperature jump of 0.1 K, which to a good approximation is within the linear regime[30]. **g**, Plotting the $R_{DS}(t)$ data as a function of the material time leads within the experimental uncertainty to the collapse predicted by the TN formalism. Note that the shapes of $R_{DLS}(\xi)$ and $R_{DS}(\xi)$ differ substantially.

subsets with the same C_{12} and C_{23}, we calculated the average C_{13} and its s.d. In Fig. 2b, the average value of C_{13} is plotted as a function of C_{12} for fixed values of C_{23} for 1P1P data measured in equilibrium, as well as after temperature jumps of different magnitudes. All data are given with s.d. as error bars that are so small that they are hardly visible (Supplementary Information). The small s.d. and the collapse of data from different temperature protocols demonstrate that C_{13} is determined by C_{12} and C_{23}, independent of the temperature protocol. Thus, Fig. 2b validates the triangular relation in and out of equilibrium.

Having confirmed a necessary condition for defining the material time via equation (1), we note that inverting equation (1) leads, for some function $\phi(x)$, to

$$\xi(t_2) - \xi(t_1) = \phi\,(C_{12})\,. \tag{4}$$

Thus, when the normalized intensity time-autocorrelation function has decayed to a certain value, a fixed amount of material time $\Delta\xi$ has elapsed. We use this to determine $\xi(t)$ in a step-by-step fashion, choosing the criterion $C(t_1, t_2) = a$ with $a = 0.3$ to define $\xi(t_2) - \xi(t_1) = \Delta\xi \equiv 1$ (other choices of a yield equivalent results; see Supplementary Information). The iterative procedure for determining the material time is illustrated in Fig. 3a using a linear time axis. The material time is defined generally by linear interpolation between its integer values. Figure 3b shows $\xi(t)$ in a log–log representation for two temperature jumps (blue and orange), as well as in equilibrium (green), where ξ is a linear function of t. In the inset $\xi(t)$ is plotted in a linear representation. Figure 3c shows the ageing rate defined by

$$\gamma \equiv \frac{\mathrm{d}\xi}{\mathrm{d}t}\,. \tag{5}$$

Following a temperature jump, γ goes from one value at the shortest times probed to the equilibrium rate at the annealing temperature.

Next we validate the TN prediction that normalized relaxation functions of a given physical quantity following different temperature jumps are identical when regarded as functions of ξ (refs. 6,9). To do this, we again consider the time-resolved correlation function of the intensity fluctuations, $C(t, t + \Delta t)$, this time however as a function of t evaluated at a constant, short lag time (here $\Delta t = 6$ s). We write in brief $C_{\Delta t}(t)$ and note that if Δt is chosen in a suitable manner, then $C_{\Delta t}(t)$ represents the change of the fluctuations during ageing. To obtain a normalized relaxation function $R_{DLS}(t)$ from $C_{\Delta t}(t)$ we define

$$R_{\mathrm{DLS}}(t) \equiv \frac{C_{\Delta t}(t) - C_{\Delta t}(t \to \infty)}{C_{\Delta t}(t = 0) - C_{\Delta t}(t \to \infty)}\,. \tag{6}$$

Figure 3d shows $R_{DLS}(t)$ as a function of time following 2 K and 4 K temperature down jumps, while Fig. 3e plots the same data as functions of the material time. The data collapse nicely in Fig. 3e, confirming the TN prediction.

Going one step further, if the TN concept is genuinely valid, the material time determined using the time evolution of any material property during ageing should collapse the relaxation function constructed from any other observable monitored during the ageing. To check this prediction, Fig. 3f shows temperature-jump data for the normalized relaxation function $R_{DS}(t)$ constructed from dielectric loss data $\varepsilon''(\nu, t)$ obtained at the frequency $\nu = 10$ kHz, while Fig. 3g shows the same data as a function of ξ. As seen in the figure, there is an almost perfect collapse of the data. Considering that the dielectric data were taken in a different laboratory, the observed small deviations are well within the experimental uncertainties. The overall conclusion from

https://doi.org/10.1038/s41567-023-02366-z

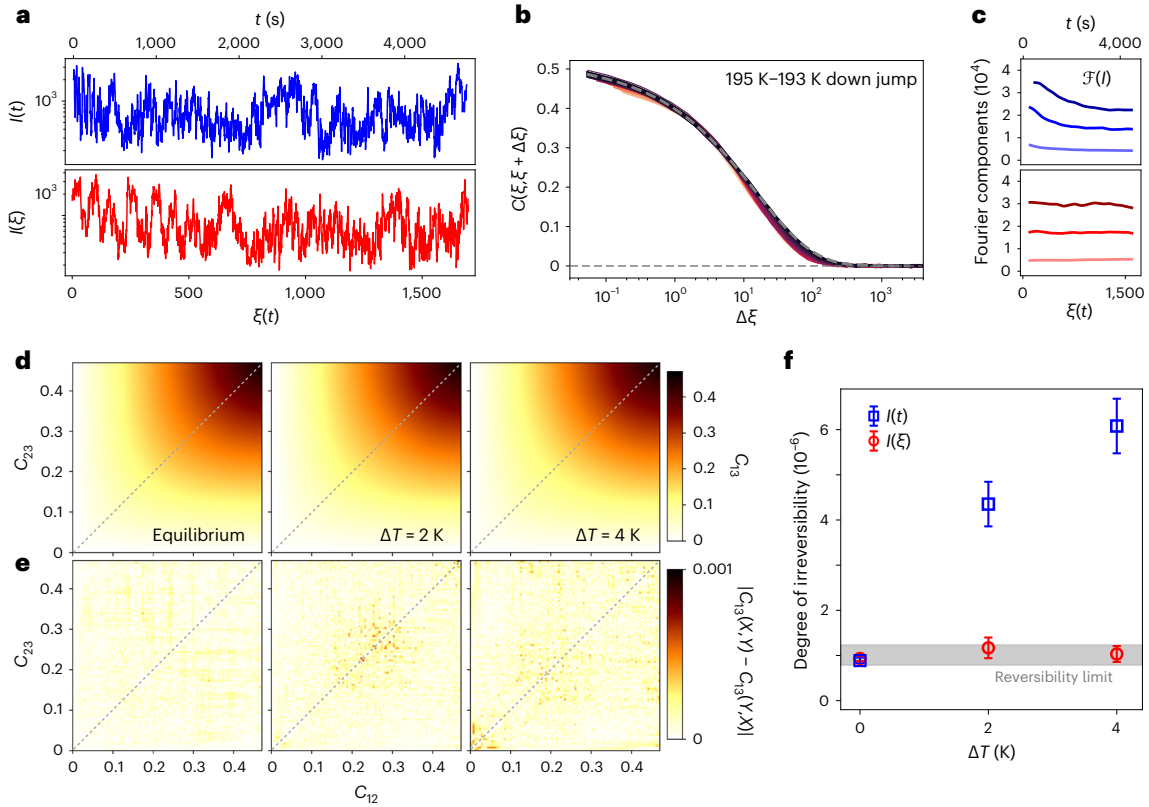

Fig. 4 | Stationarity and reversibility of the intensity fluctuations regarded as functions of the material time. a, Light-scattering intensity in one exemplary speckle for a $\Delta T = 4$ K down jump to 193 K analysed at equally spaced time intervals or material-time intervals. **b**, The time-autocorrelation functions of Fig. 1e parameterized by the starting material time $\xi(t)$, plotted as a function of $\Delta\xi(t)$. The fact that the data collapse onto one curve shows that fluctuations during physical ageing are stationary functions of ξ. **c**, Moving time-window Fourier components of the intensity at three frequencies plotted as a function of time (upper panel) and material time (lower panel). A systematic time dependence is observed in the former case, while the Fourier components are virtually constant as functions of the material time, confirming stationarity. **d**, C_{13} indicated by the colours for given values of C_{12} and C_{23} that define the x and y axes, respectively. Data are given for equilibrium and two temperature down jumps to 193 K. The diagonal symmetry confirms equation (3). **e**, Quantification of of deviations from reversibility $|C_{13}(X, Y) - C_{13}(Y, X)|$, which is in all cases very small. **f**, Comparison of the degree of irreversibility for the intensity time series considered as functions of t and ξ, quantified by the Jensen–Shannon divergence of the average visibility-graph degree distributions[45,46] averaged over 10^4 time series. Each point reflects the mean value ± s.d. of $n = 10$ statistically independent analyses. The larger this quantity is, the more irreversible is the time series in question. Note that zero can only be reached for an infinitely long reversible time series; the grey 'reversibility limit' was identified by surrogate data testing[68] performing the same analysis on a set of artificially generated reversible time series of the same statistics and length as the actual data time series (Methods).

Fig. 3d–g is that the TN material time identified from the light-scattering intensity time-autocorrelation function leads to a linear behaviour when the relaxation during ageing is considered as a function of the material time, independent of the particular observable used to monitor the ageing process. This confirms that the material time has been identified correctly.

Material-time stationarity and reversibility

Having shown how to determine the material time during physical ageing from the normalized DLS intensity time-autocorrelation function, we now turn to this paper's central question: whether the linearization obtained by replacing time with material time translates into statistical reversibility of the intensity fluctuations.

Stationarity of a stochastic process is a necessary condition for reversibility[44]. The three top panels of Fig. 4 investigate to what degree the intensity fluctuations are stationary when regarded as functions of the material time for a jump from equilibrium at 197 K to equilibrium at 193 K. Figure 4a shows the intensity data probed in one exemplary speckle as a function of t (blue) and ξ (red). Although the figures differ visibly, it is not immediately clear whether the lower data are more stationary than the upper. To investigate this we consider in Fig. 4b the material-time based correlation function of the speckle-averaged fluctuations, $C(\xi, \xi + \Delta\xi)$. This is found to be independent of ξ, meaning that $C(\xi, \xi + \Delta\xi)$ is material-time-translation invariant and thus stationary. Figure 4c illustrates the same aspect in the frequency domain by determining the Fourier components at three frequencies (for fixed-length moving time, respectively, material-time windows) and demonstrates that these become constant as functions of the material time (full spectrograms are shown in Supplementary Information).

After validating stationarity of the $I(\xi)$ time series, the lower panels of Fig. 4 investigate whether reversibility applies in the sense that time series of intensity fluctuations have the same statistics as the time-reversed series. Figure 4d shows data for the normalized intensity time-autocorrelation function in equilibrium and for physical ageing in a heat map showing $C_{13} \equiv C(t_1, t_3)$ as a function of C_{12} and C_{23}. The diagonal symmetry confirms the reversibility condition equation (3). The degree of deviations from symmetry for given values of $X = C_{12}$ and $Y = C_{23}$, $|C_{13}(X, Y) - C_{13}(Y, X)|$, is investigated in Fig. 4e, which shows deviations smaller than 1‰. A different test of material-time reversibility is given in Fig. 4f, where we apply the visibility-graph algorithm[45] to the intensity time series. This algorithm is well suited for our data as it works scale free and assesses 'global' aspects of reversibility[46]. The idea is to map the time series onto a directed graph with nodes representing the time-series element edges defined according to a geometric criterion, how far one can 'see' along the time axis[45]. If a given time series is reversible, the visibility graph has the same statistical

https://doi.org/10.1038/s41567-023-02366-z

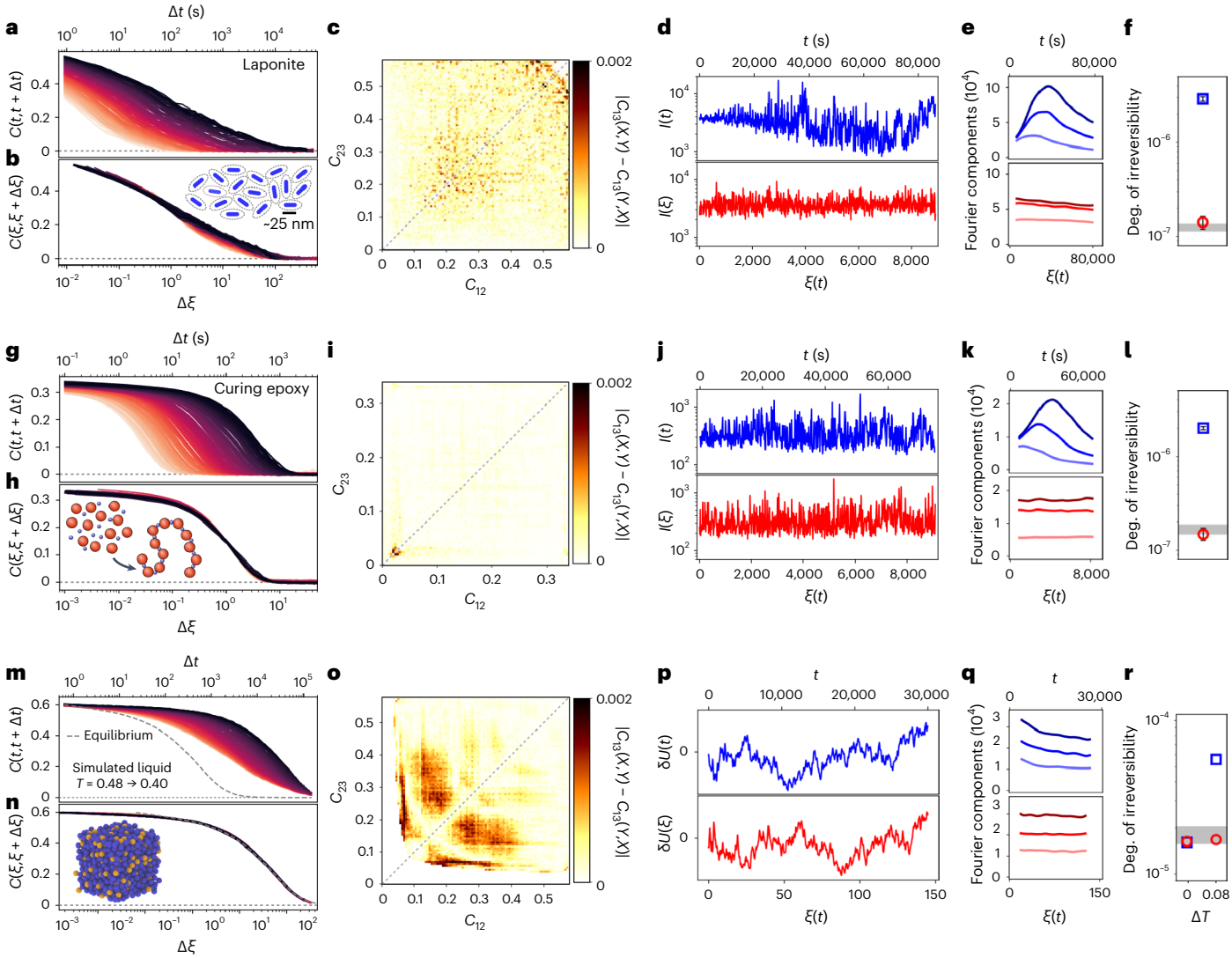

Fig. 5 | Physical ageing data for the colloidal glass-former Laponite, chemical ageing data for a linear polymerizing epoxy and computer simulation data for a binary LJ system. a–**f**, Data for disc-shaped Laponite particles dissolved in deionized water, which gradually solidify into a colloidal glass. **g**–**l**, Linear polymerization of bisphenol A diglycidyl ether initiated upon mixing with appropriate linker molecules. **m**–**r**, Ageing of the potential-energy fluctuations of a binary LJ mixture after a temperature down jump from 0.48 to 0.40. Here temperatures and times are expressed using the respective dimensionless LJ units. Each row displays the same analyses applied to each system. In the following discussion, we refer to the panel labels in the order: Laponite, epoxy, LJ. **a**,**g**,**m**, Slowdown of time-autocorrelation functions as the annealing time increases. **c**,**i**,**o**, Heat maps analogous to those of Fig. 4e confirming material-time reversal invariance. The necessary condition of stationarity of the intensity time series (**d**,**j**,**p**) with regard to the material time (red) is confirmed for the corresponding Fourier components in **e**,**k**,**q** and for the time-autocorrelation functions in **b**,**h**,**n**. **f**,**l**,**r**, Results analogous to those of Fig. 4f. In **f** and **l**, each point reflects the mean ± s.d. of $n = 10$ statistically independent analyses. Note that **r** also includes data for an equilibrium simulation ($\Delta T = 0$).

properties as the time-reversed one. This can be tested by comparing their respective degree distributions using an appropriate statistical measure—for example, the Jensen–Shannon divergence[47]. Figure 4f shows this measure of the degree of irreversibility for the $I(t)$ and $I(\xi)$ fluctuations (blue and red, respectively), where $\Delta T = 0$ gives the equilibrium data. The grey area marks the lower range of values that can be obtained for a finite time series, as only for an infinite reversible time series can one obtain a zero Jensen–Shannon divergence. We conclude that, within the experimental resolution, the physical ageing of 1P1P leads to scattered-light intensity fluctuations that are statistically reversible when regarded as functions of the material time, while they are clearly irreversible as functions of time.

Results for other systems

To test the generality of the above findings we also investigated Laponite, a colloidal system of synthetic 25-nm-sized disc-shaped clay particles that after stirring in water solidifies gradually into a transparent colloidal glass[48]. In this case we cannot probe the full approach to equilibrium, because the system keeps solidifying within any realistic time window of observation. Nevertheless, following the above procedure we can define a material time from the normalized scattered-light intensity time-autocorrelation function. To vary the experimental conditions, we changed from depolarized (VH) to polarized (VV) light-scattering geometry, which probes local particle-density fluctuations[31].

The results for Laponite are summarized in the top panels of Fig. 5, in which Fig. 5a shows data for the normalized intensity time-autocorrelation function. Clearly, the particle dynamics slows considerably during the experiment. Material-time stationarity is validated in Fig. 5b, while Fig. 5c confirms the symmetry of $C_{13}(C_{23}, C_{12})$, analogous to Fig. 4e, thus demonstrating material-time reversibility. There is not a perfect data collapse in Fig. 5b, but it should be noted that

these data cover more than two decades of relaxation times. Possibly, a fast microscopic process[49] or a decoupling of translational and rotational degrees of freedom[50] could lead to slight deviations from perfect stationarity. Figure 5d shows the intensity time and material-time series of one exemplary speckle. The amplitudes of the fluctuations as functions of t and ξ differ visibly as a consequence of the averaging over exposure time intervals that are fixed in regard to t or ξ, respectively; see Supplementary Information for a detailed discussion of this. The effect is most pronounced for the Laponite data due to the large change of the relaxation time during ageing. Finally, Fig. 5e shows three of the respective Fourier components evaluated over moving time windows, while Fig. 5f demonstrates material-time reversibility following the same procedure as in Fig. 4f.

Our work set out to investigate whether material-time reversibility is a characteristic of physical ageing. Having confirmed this for two quite different systems, we searched for a counterexample and decided to investigate an irreversibly reacting chemical system, namely the linearly polymerizing epoxy based on bisphenol A diglycidyl ether (Methods). We monitored the dynamics during polymerization by VH depolarized light scattering. The results are shown in the middle panels of Fig. 5, which are analogous to those of Laponite. Surprisingly, no counterexample to material-time reversibility is provided by this chemically ageing system; in fact the findings are very similar to those of physically ageing systems in terms of demonstrating stationarity in Fig. 5k, collapse of correlation functions in Fig. 5h and material-time reversibility in Fig. 5i,l.

Finally, we simulated a modification of the Kob–Andersen binary Lennard-Jones (LJ) model of a supercooled liquid[51,52] following a temperature down jump from a state of equilibrium. The quantity monitored during ageing is the instantaneous value of the potential energy of each particle (Methods). The same analysis as for the experimental data was carried out for the per-particle potential energy, demonstrating the generality of our findings in Fig. 5m–r. The per-particle potential-energy fluctuation time-autocorrelation functions are shown in Fig. 5m as a function of time. These collapse almost perfectly as functions of the material time in Fig. 5n. Material-time reversibility is tested in Fig. 5o, where minor deviations from perfect symmetry are observed. For further testing reversibility we studied time series reflecting the summed potential-energy fluctuations of 200 randomly chosen particles, δU. The resulting degrees of irreversibility are shown in Fig. 5r, where $\delta U(\xi)$ is shown to be just as reversible as $\delta U(t)$ of the equilibrium liquid at the annealing temperature. This result was obtained after applying a narrow Gaussian filter to eliminate the fast microscopic fluctuations, which otherwise lead to a subtle residual irreversibility in $\delta U(\xi)$ (see Discussion, Methods and Supplementary Information).

Discussion

We have presented ageing data for a supercooled molecular liquid obtained by multispeckle depolarized DLS. By averaging over a multitude of speckles, time-resolved intensity time-autocorrelation functions can be determined with good accuracy during ageing. This presents a distinct advantage over other experimental approaches used to monitor the dynamics of ageing. Our approach allows a detailed analysis of the shape of time-autocorrelation functions during ageing, including when the timescales of ageing and the observed correlation decay are similar.

We used the light-scattering data to validate the material-time concept of the TN formalism. This concept, which has been applied successfully for half a century to describe physical ageing[6,9,13,17], is remarkable in terms of transforming a highly nonlinear phenomenon into a linear one simply by replacing time with material time. Since standard linear-response theory reflects the time reversibility of the fundamental laws of physics, this suggests that fluctuations during physical ageing are statistically reversible when regarded as functions of the material time. We validated this for light-scattering data on three ageing systems—1P1P, Laponite and a curing epoxy—as well as for data on a computer-simulated ageing LJ model liquid. Note that these systems differ in several respects: 1P1P and epoxy are molecular while Laponite is colloidal; 1P1P, Laponite and LJ age physically while epoxy ages chemically; Laponite and epoxy do not converge to equilibrium within the window of observation while 1P1P and LJ do. Moreover, our experiments probed dynamics on different length scales: while reorientation of the optical anisotropy on a molecular scale is probed in VH light scattering of 1P1P, in the case of VV scattering on Laponite density fluctuations are probed on the scale of the optical wavelength. In VH scattering of the curing epoxy, it is mainly hardener/resin concentration fluctuation effects that are probed. Finally, similarly to 1P1P, the computer simulations access the single-particle scale. Despite these notable differences, all four systems obey the triangular relation equation (2) and have fluctuations that within the experimental resolution are stationary and reversible when considered as functions of the material time.

It is important to emphasize that, while we have demonstrated material-time reversibility of the light-scattering intensity statistics on the timescale of the structural relaxation, the description in terms of a material time does not necessarily lead to reversibility of the microscopic dynamics in the picosecond range. Such fast dynamics are found in almost all glassy materials, however are virtually unaffected by ageing, which is why they can not be expected to conform to the concept of a material time. Moreover, even when the light-scattering intensity fluctuations are material-time reversible, other quantities may well show irreversible behaviour. This caveat has recently been discussed by O'Byrne and co-workers in connection with the dynamics of active matter[53], demonstrating that, while the microscopic dynamics of active matter is not time reversible, the dynamics of observables referring to the coarse-grained level may appear so. Since establishing absolute reversibility involves testing infinitely many different variables, it cannot be excluded that our ageing samples are irreversible at some deeper level. To investigate this in the future, a promising approach would be to analyse light-scattering and other data using machine-learning techniques, as recently suggested by Seif et al.[54].

In view of our findings the question arises of whether the material time determined by one specific method, say DLS, uniquely determines the transient state of the ageing system[9,13], that is, whether all other observables probing ageing become linear and the corresponding fluctuations become stationary and time reversible when considered as a function of the material time. We elucidate these questions by showing that relaxation functions constructed from dielectric data do indeed become linear using the DLS material time (Fig. 3g). Whether this holds in general and includes other static and dynamic observables remains an open question[55]. We note that results from different linear-response experiments show that, at least for some glass-forming liquids, the ratio of relaxation times of different quantities is independent of the temperature[56], which is consistent with the existence of a unique material time.

While the concept of reversibility is fundamental in physics, in the present context we considered it more generally as a formal time-series property, as, for example, recently discussed in connection with neuroscience[57]. We are not aware of a theoretical framework that predicts material-time statistical reversibility of fluctuations during ageing. The TN ageing description is phenomenological and has no predictions for fluctuations. Assuming in the TN spirit that the intensity time-autocorrelation function during ageing is a function of the material-time increase, the triangular relation equation (2) and the symmetry relation equation (3) were derived above. In that approach these identities may be regarded as inherited from thermal equilibrium. Equations (2) and (3) were originally derived, however, by Cugliandolo and Kurchan in an entirely different context[33,58]. Cugliandolo and Kurchan studied spin models with infinite-range interactions and showed that the exact Schwinger–Dyson equations for fluctuation and response imply equations (2) and (3) at low temperatures where

the system never converges to equilibrium. At higher temperatures, on the other hand, the system converges to equilibrium and no triangular relation was predicted. Under the latter conditions, however, we do find that the triangular relation applies, as shown above for 1P1P and the computer simulations of simple LJ type systems ageing to equilibrium[42,43]. The Cugliandolo–Kurchan mean-field approach is exact in infinite dimensions[33,59]. Although the basic Cugliandolo–Kurchan predictions were later proposed to apply also in finite dimensions[42,60], the range of applicability of the mean-field scenario remains unclear[16]. Interestingly, the subject of time-reparametrization invariance pioneered by Cugliandolo and Kurchan[33], which is a consequence of the triangular relation, has recently become fashionable in field theory, where it represents the 'gravity' low-energy limit[61,62].

Our results give rise to a number of questions: whether material-time reversibility is a universal characteristic of ageing; whether it is possible to formulate generalized fluctuation–dissipation relations based on material time instead of laboratory time, possibly on a coarse-grained level, and if so, how this would relate to the effective-temperature concept introduced long ago for the description of ageing[63]; whether material-time reversibility reflects the reversibility of the fundamental laws of physics and thereby connects to the fluctuation theorem that quantifies a consequence of microscopic time reversibility[64,65]. To illuminate these questions it would be interesting to find an ageing system that violates material-time reversibility, but we have so far failed to do so. Possibly, this could be achieved by performing large temperature jumps, as suggested by recent results[66,67].

Online content

Any methods, additional references, Nature Portfolio reporting summaries, source data, extended data, supplementary information, acknowledgements, peer review information; details of author contributions and competing interests; and statements of data and code availability are available at https://doi.org/10.1038/s41567-023-02366-z.

References

1. Rovelli, C. *The Order of Time* (Penguin Books, 2018).
2. Landau, L. D. and Lifshitz, E. M. *Statistical Physics* (Pergamon, 1958).
3. Reichl, L. E. *A Modern Course in Statistical Physics* 4th edn (Wiley-VCH, 2016).
4. Onsager, L. Reciprocal relations in irreversible processes. II. *Phys. Rev.* **38**, 2265–2279 (1931).
5. Tool, A. Q. Relation between inelastic deformability and thermal expansion of glass in its annealing range. *J. Am. Ceram. Soc.* **29**, 240–253 (1946).
6. Narayanaswamy, O. S. A model of structural relaxation in glass. *J. Am. Ceram. Soc.* **54**, 491–498 (1971).
7. Mandal, R., Tapias, D. & Sollich, P. Memory in non-monotonic stress response of an athermal disordered solid. *Phys. Rev. Res.* **3**, 043153 (2021).
8. Struik, L. C. E. *Physical Aging in Amorphous Polymers and Other Materials* (Elsevier, 1978).
9. Scherer, G. W. *Relaxation in Glass and Composites* (Wiley, 1986).
10. Hodge, I. M. Physical aging in polymer glasses. *Science* **267**, 1945–1947 (1995).
11. Chen, K. & Schweizer, K. S. Molecular theory of physical aging in polymer glasses. *Phys. Rev. Lett.* **98**, 167802 (2007).
12. Micoulaut, M. Relaxation and physical aging in network glasses: a review. *Rep. Prog. Phys.* **79**, 066504 (2016).
13. McKenna, G. B. & Simon, S. L. 50th anniversary perspective: Challenges in the dynamics and kinetics of glass-forming polymers. *Macromolecules* **50**, 6333–6361 (2017).
14. Ruta, B., Pineda, E. & Evenson, Z. Relaxation processes and physical aging in metallic glasses. *J. Phys. Condens. Matter* **29**, 503002 (2017).
15. Cangialosi, D. *Physical Aging of Polymers* (Wiley, 2018).
16. Arceri, F., Landes, F.P., Berthier, & L., Biroli, G. in *Statistical and Nonlinear Physics. Encyclopedia of Complexity and Systems Science Series* (ed. Chakraborty, B.) 229–296 (Springer, 2022).
17. McKenna, G. B. On the physics required for prediction of long term performance of polymers and their composites. *J. Res. Natl Inst. Stand. Technol.* **99**, 169–189 (1994).
18. Monnier, X., Cangialosi, D., Ruta, B., Busch, R. & Gallino, I. Vitrification decoupling from α-relaxation in a metallic glass. *Sci. Adv.* **6**, eaay1454 (2020).
19. Zhao, Y. et al. Ultrastable metallic glass by room temperature aging. *Sci. Adv.* **8**, eabn3623 (2022).
20. Simon, F. Über den Zustand der unterkühlten Flüssigkeiten und Gläser. *Z. Anorg. Allg. Chem.* **203**, 219–227 (1931).
21. Roth, C. B. (ed.) *Polymer Glasses* (CRC Press, 2017).
22. Lulli, M., Lee, C.-S., Deng, H.-Y., Yip, C.-T. & Lam, C.-H. Spatial heterogeneities in structural temperature cause Kovacs' expansion gap paradox in aging of glasses. *Phys. Rev. Lett.* **124**, 095501 (2020).
23. Mandal, R. & Sollich, P. Multiple types of aging in active glasses. *Phys. Rev. Lett.* **125**, 218001 (2020).
24. Pastore, R., Siviello, C. & Larobina, D. Elastic and dynamic heterogeneity in aging alginate gels. *Polymers* **13**, 3618 (2021).
25. Janzen, G. & Janssen, L. M. C. Aging in thermal active glasses. *Phys. Rev. Res.* **4**, L012038 (2022).
26. Schober, H. R. Diffusion, relaxation, and aging of liquid and amorphous selenium. *Phys. Rev. B* **103**, 094202 (2021).
27. Elizondo-Aguilera, L. F., Rizzo, T. & Voigtmann, T. From subaging to hyperaging in structural glasses. *Phys. Rev. Lett.* **129**, 238003 (2022).
28. Kob, W. & Barrat, J.-L. Fluctuations, response and aging dynamics in a simple glass-forming liquid out of equilibrium. *Eur. Phys. J. B* **13**, 319–333 (2000).
29. Kovacs, A. J., Aklonis, J. J., Hutchinson, J. M. & Ramos, A. R. Isobaric volume and enthalpy recovery of glasses. II. A transparent multiparameter theory. *J. Polym. Sci. Polym. Phys.* **17**, 1097–1162 (1979).
30. Riechers, B. et al. Predicting nonlinear physical aging of glasses from equilibrium relaxation via the material time. *Sci. Adv.* **8**, eabl9809 (2022).
31. Berne, B. J. and Pecora, R. *Dynamic Light Scattering: with Applications to Chemistry, Biology, and Physics* (Wiley, 1976).
32. Riechers, B. & Richert, R. Rate exchange rather than relaxation controls structural recovery. *Phys. Chem. Chem. Phys.* **21**, 32–37 (2019).
33. Cugliandolo, L. F. & Kurchan, J. On the out-of-equilibrium relaxation of the Sherrington–Kirkpatrick model. *J. Phys. A* **27**, 5749–5772 (1994).
34. Viasnoff, V. & Lequeux, F. Rejuvenation and overaging in a colloidal glass under shear. *Phys. Rev. Lett.* **89**, 065701 (2002).
35. Cipelletti, L., Bissig, H., Trappe, V., Ballesta, P. & Mazoyer, S. Time-resolved correlation: a new tool for studying temporally heterogeneous dynamics. *J. Phys. Condens. Matter* **15**, S257 (2002).
36. Kaloun, S., Skouri, M., Knaebel, A., Münch, J.-P. & Hébraud, P. Aging of a colloidal glass under a periodic shear. *Phys. Rev. E* **72**, 011401 (2005).
37. Li, Q., Peng, X. & McKenna, G. B. Long-term aging behaviors in a model soft colloidal system. *Soft Matter* **13**, 1396–1404 (2017).
38. Aime, S., Ramos, L. & Cipelletti, L. Microscopic dynamics and failure precursors of a gel under mechanical load. *Proc. Natl Acad. Sci. USA* **115**, 3587–3592 (2018).
39. Ruta, B. et al. Atomic-scale relaxation dynamics and aging in a metallic glass probed by X-ray photon correlation spectroscopy. *Phys. Rev. Lett.* **109**, 165701 (2012).

40. Evenson, Z. et al. X-ray photon correlation spectroscopy reveals intermittent aging dynamics in a metallic glass. *Phys. Rev. Lett.* **115**, 175701 (2015).
41. Cornet, A. et al. Denser glasses relax faster: Enhanced atomic mobility and anomalous particle displacement under in-situ high pressure compression of metallic glasses. *Acta Mater.* **255**, 119065 (2023).
42. Avila, K. E., Castillo, H. E. & Parsaeian, A. Fluctuations in the time variable and dynamical heterogeneity in glass-forming systems. *Phys. Rev. E* **88**, 042311 (2013).
43. Douglass, I. M. & Dyre, J. C. Distance-as-time in physical aging. *Phys. Rev. E* **106**, 054615 (2022).
44. Lawrance, A. J. Directionality and reversibility in time series. *Int. Stat. Rev.* **59**, 67–79 (1991).
45. Lacasa, L., Luque, B., Ballesteros, F., Luque, J. & Nuno, J. C. From time series to complex networks: the visibility graph. *Proc. Natl Acad. Sci. USA* **105**, 4972–4975 (2008).
46. Lacasa, L., Nunez, A., Roldán, E., Juan, J. M. R. & Luque, B. Time series irreversibility: a visibility graph approach. *Eur. Phys. J. B* **85**, 217 (2012).
47. Menéndez, M. L., Pardo, J. A., Pardo, L. & Pardo, M. C. The Jensen–Shannon divergence. *J. Franklin Inst.* **334**, 307–318 (1997).
48. Ruzicka, B. & Zaccarelli, E. A fresh look at the Laponite phase diagram. *Soft Matter* **7**, 1268–1286 (2011).
49. Augusto de Melo Marques, F. et al. Structural and microscopic relaxations in a colloidal glass. *Soft Matter* **11**, 466–471 (2015).
50. Jabbari-Farouji, S., Zargar, R., Wegdam, G. H. & Bonn, D. Dynamical heterogeneity in aging colloidal glasses of Laponite. *Soft Matter* **8**, 5507–5512 (2012).
51. Kob, W. & Andersen, H. C. Testing mode-coupling theory for a supercooled binary Lennard-Jones mixture I: the Van Hove correlation function. *Phys. Rev. E* **51**, 4626–4641 (1995).
52. Toxvaerd, S., Pedersen, U. R., Schrøder, T. B. & Dyre, J. C. Stability of supercooled binary liquid mixtures. *J. Chem. Phys.* **130**, 224501 (2009).
53. O'Byrne, J., Kafri, Y., Tailleur, J. & van Wijland, F. Time-(ir) reversibility in active matter, from micro to macro. *Nat. Rev. Phys.* **4**, 167–183 (2022).
54. Seif, A., Hafezi, M. & Jarzynski, C. Machine learning the thermodynamic arrow of time. *Nat. Phys.* **17**, 105–113 (2021).
55. Peredo-Ortiz, R., Medina-Noyola, M., Voigtmann, T. & Elizondo-Aguilera, L. F. Inner clocks of glass-forming liquids. *J. Chem. Phys.* **156**, 244506 (2022).
56. Roed, L. A., Dyre, J. C., Niss, K., Hecksher, T. & Riechers, B. Time-scale ordering in hydrogen- and van der Waals-bonded liquids. *J. Chem. Phys.* **154**, 184508 (2021).
57. Kringelbach, M. L., Perl, Y. S., Tagliazucchi, E. & Deco, G. Toward naturalistic neuroscience: mechanisms underlying the flattening of brain hierarchy in movie-watching compared to rest and task. *Sci. Adv.* **9**, eade6049 (2023).
58. Chamon, C. & Cugliandolo, L. F. Fluctuations in glassy systems. *J. Stat. Mech.* **7**, P07022 (2007).
59. Agoritsas, E., Maimbourg, T. & Zamponi, F. Out-of-equilibrium dynamical equations of infinite-dimensional particle systems I. The isotropic case. *J. Phys. A* **52**, 144002 (2019).
60. Castillo, H. E. & Parsaeian, A. Local fluctuations in the ageing of a simple structural glass. *Nat. Phys.* **3**, 26–28 (2007).
61. Facoetti, D., Biroli, G., Kurchan, J. & Reichman, D. R. Classical glasses, black holes, and strange quantum liquids. *Phys. Rev. B* **100**, 205108 (2019).
62. Kurchan, J. Time-reparametrization invariances, multithermalization and the Parisi scheme. *SciPost Phys. Core* **6**, 001 (2023).
63. Cugliandolo, L. F. The effective temperature. *J. Phys. A* **44**, 483001 (2011).
64. Bochkov, G. N. & Kuzovlev, Yu. E. Nonlinear fluctuation–dissipation relations and stochastic models in nonequilibrium thermodynamics. I. Generalized fluctuation–dissipation theorem. *Physica A* **106**, 443–479 (1981).
65. Evans, D. J. & Searles, D. J. The fluctuation theorem. *Adv. Phys.* **51**, 1529–1585 (2002).
66. Cangialosi, D., Boucher, V. M., Alegría, A. & Colmenero, J. Direct evidence of two equilibration mechanisms in glassy polymers. *Phys. Rev. Lett.* **111**, 095701 (2013).
67. Herrero, C., Scalliet, C., Ediger, M. D. & Berthier, L. Two-step devitrification of ultrastable glasses. *Proc. Natl Acad. Sci. USA* **120**, e2220824120 (2023).
68. Schreiber, T. & Schmitz, A. Surrogate time series. *Physica D* **142**, 346–382 (2000).

Methods

Multispeckle DLS set-up and temperature protocols

Experiments are performed in a custom-built light-scattering set-up, where a Cobolt Samba 500 Nd:YAG laser (wavelength 532 nm) is used to illuminate the sample with vertically polarized light. The sample cell is mounted inside a CryoVac cold-finger cryostat surrounded by a high vacuum generated by a vibration-free Agilent ion getter pump. Scattered light is detected at 90° angle using a Hamamatsu ORCA-Flash 4.0 V2 sCMOS camera. Light is guided onto the camera chip by a custom-built optical system consisting of a circular aperture, an $f = 6$ cm spherical lens, a finely adjustable Glan–Thompson polarizer from B. Halle with extinction ratio 10^{-6}, an adjustable slit aperture and a 2 nm band-pass filter (in the order towards the detection unit).

To calibrate the temperature protocols, the sample temperature must be monitored precisely. This has been achieved by constructing a dummy sample cell of the same geometry as the original light-scattering cell, but equipped with two PT100 temperature sensors: the first one is located inside the liquid sample, the second one is glued into a channel drilled through the aluminium bottom of the sample cell using Loctite Stycast 2850FT thermally conducting epoxy glue. During the light-scattering measurements only the second sensor could be used, as positioning a sensor inside the liquid interferes with the laser beam. Using the dummy sample cell it was confirmed that the two sensors coincide for different temperature protocols, implying that the temperature determined by the second sensor is an appropriate measure of the actual sample temperature.

To perform a fast temperature down jump from the starting temperatures $T_0 = 197$ K, 195 K to the annealing temperature $T_\infty = 193$ K with amplitude $\Delta T = T_0 - T_\infty$ it is not sufficient to simply quench the cold finger from T_0 to T_∞ and let the sample equilibrate there. Due to the thermal lag between cold finger and sample cell, the sample temperature initially decreases quickly, but as soon as the cold finger reaches T_∞ the cooling rate inside the sample declines and it takes more than 1,000 s for the sample temperature to reach T_∞. To mitigate this we initially cooled the cold finger several degrees below T_∞ as quickly as possible. This temperature was then held for a short time t, after which the cold finger was heated back to T_∞ with heating rate c. By choosing t and c in an optimal way, it was possible to have the sample temperature quickly reach T_∞ without any relevant temperature undershoot (see Supplementary Information for details). The parameters for the optimal temperature protocol were determined for $\Delta T = 0.5$, 1.0, 2.0 and 4.0 K before the light-scattering measurements (0.5 and 1.0 K are not shown, but used for the analysis in Fig. 3g). We limit the study to these temperature-jump amplitudes because larger temperature jumps would require higher cooling rates that cannot be obtained with the present set-up. During the measurements, the prepared temperature protocols were repeated, and reproducibility was ensured by controlling the Lakeshore 335 temperature controller via Python scripts. Following this procedure, temperature jumps could be performed in less than 200 s with an accuracy of 0.1 K. The final temperature could then be held for >24 h with an accuracy of ±0.05 K.

Sample preparation and measurements

1P1P. 1P1P (Alfa Aesar, 98+% purity) was filtered into the light-scattering sample cell using a 450 nm syringe filter. The sample was first kept at T_0 for 12 h to ensure that the supercooled liquid was in (metastable) thermal equilibrium. A camera measurement quantifying the equilibrium state at T_0 was performed with exposure time 0.02 s over 300,000 frames (6,000 s). After this, a second camera measurement was started with an exposure time of 0.2 s over 300,000 frames (~17 h). Simultaneously, the prepared temperature protocol was initiated. The duration of the measurement was chosen to be much longer than the time needed for the sample to equilibrate, which allowed us to analyse in detail the equilibrium intensity fluctuations. All experiments involving 1P1P were performed in the VH (depolarized) geometry, thus the reorientation of the molecular optical anisotropy tensor is probed[31].

For the dielectric measurements the complex capacity was measured at the fixed frequency $\nu_0 = 10$ kHz, with an Andeen-Hagerling AH 2700A high-precision bridge in a custom-built cryostat system[69,70]. Fast temperature jumps up to $\Delta T = 4$ K with microkelvin precision were obtained by a subcryostat system based on a Peltier element and a nonlinear temperature sensor[69,71]. The sample temperature can be changed in a few seconds.

From the complex capacity, the complex permittivity of 1P1P at 10 kHz was determined and its imaginary part, $\varepsilon''(t)$, was used to calculate $R_{DS}(t)$ analogous to equation (6),

$$R_{DS}(t) = \frac{\varepsilon''(t) - \varepsilon''(t \to \infty)}{\varepsilon''(t=0) - \varepsilon''(t \to \infty)}. \quad (7)$$

Data were collected linearly in time and averaged using a logarithmic binning scheme. To combine DLS and DS measurements we account for slight differences regarding the annealing temperature, which inevitably appear due to the experiments being performed in different laboratories. We determine the respective relaxation time at the annealing temperatures of both experiments by considering the results from a detailed analysis of 1P1P using both methods in ref. 72 and apply the procedure presented in Supplementary Section 1 to determine the temperature difference.

Laponite. The Laponite suspension was prepared in consideration of the phase diagram[73] with parameters chosen such that a colloidal Wigner glass was obtained: Laponite powder (Laponite-RD from BYK) was dried for one week at 1 mbar to remove all water. Water with pH 10 and ionic strength < 10^{-4} M was obtained by adding an appropriate amount of NaOH to milli-Q water. Subsequently, 2.98 wt% of Laponite was added and the mixture was stirred for 24 h. Finally, the sample was filtered into a glass cylinder using a 450 nm syringe filter, which may have led to a slight reduction of the Laponite concentration. Physical ageing starts directly after the mixture is filtered; however, for the first few hours the colloidal dynamics is too fast to be captured by the camera. The camera measurement with exposure time 0.1 s was started several minutes after filtration, and the scattered light was monitored in VV geometry over 1,500,000 frames (~42 h). Laponite was studied at room temperature.

Epoxy. The epoxy system is based on bisphenol A diglycidyl ether resin (Alfa Aesar). As polymerization agent we used *N*,*N*,*N*′,*N*′-tetraethyldiethylenetriamine (Sigma Aldrich, 90%). This specific agent induces a linear polymerization; thus the mixture was prepared with a 1:1 molar ratio. Before mixing, the resin was dried and degassed in a vacuum oven. Afterwards, a glass syringe equipped with a stainless steel filter holder containing a 450 nm nylon membrane filter suitable for operation at high temperatures was filled with the resin. The syringe was then heated to 150 °C to decrease the viscosity of the resin, which allowed us to filter the resin into a dust-free sample glass. The appropriate amount of hardener was added, again using a syringe filter. Subsequently, the mixture was magnetically stirred at 400 r.p.m. for 10 min and a dust-free cylindrical glass sample holder was filled with the mixture. Air bubbles were removed by exposing it to vacuum for 15 min. Finally, the glass tube was sealed and placed inside a suitable sample oven preheated to 310 K, and the camera measurement in VH geometry with exposure time 0.1 s was started for 2,000,000 frames (~56 h).

Molecular dynamics

The data for the binary LJ system presented in Fig. 5 were produced using the graphics processing unit (GPU)-optimized software RUMD[74]. The interaction potential used is the modification of the standard Kob–Andersen potential introduced in ref. 75 to counteract crystallization.

Jumps from temperature 0.48 to 0.40 at density 1.20 for a system of $N = 8{,}000$ particles (6,400 A particles and 1,600 B particles) were simulated for 1.68×10^5 LJ time units with a time step of 0.005. The simulations ran in the *NVT* ensemble using a standard Nosé-Hoover thermostat with relaxation time 0.2 in LJ units. Velocities were rescaled at the start of the simulation to temperature 0.40 to avoid non-physical behaviour of the thermostat. The potential energy of each particle was saved every 128 time steps (corresponding to 0.64 LJ time units). Simulations from 30 independent starting configurations were run. The data shown in Fig. 5 refer to the A particles only and consider a total of 192,000 particles to obtain time-autocorrelation functions with minimal statistical noise. Starting configurations were obtained from an equilibrium simulation at density 1.20 and temperature 0.48, separated in time by 4.2×10^4 LJ units (roughly corresponding to 80 relaxation times).

Data analysis

For all temperature jumps of 1P1P, for Laponite during annealing and for the curing epoxy, the resulting camera video files were analysed using three different techniques to obtain time-resolved autocorrelation functions, pairwise autocorrelations for time triplets and intensity time series as a function of t and ξ. The same procedures were used to analyse the simulation data. In the following, each procedure and subsequent analyses are explained.

Time-resolved autocorrelation functions. Time-resolved autocorrelation functions were obtained from the camera video via a multipixel average over images consisting of $n = 2{,}048$ columns and $m = 350$ rows. Due to the Gaussian intensity profile of the laser beam, the average pixel intensity varies slightly perpendicular to the propagation direction of the laser (respectively for different rows). At the same time, the average intensity is constant along the propagation direction (respectively for different columns). Thus, normalization of autocorrelations is carried out independently for each row. Finally, the result is averaged over all rows. Mathematically, our procedure amounts to

$$C(t, t+\Delta t) = \frac{n}{m}\sum_{j=1}^{m}\left[\frac{\sum_{i=1}^{n} I_{ij}(t) I_{ij}(t+\Delta t)}{\left(\sum_{i=1}^{n} I_{ij}(t)\right)\left(\sum_{i=1}^{n} I_{ij}(t+\Delta t)\right)}\right] - 1, \tag{8}$$

with column i and row j. $C(t, t+\Delta t)$ was calculated for all available t (each frame) and for 47 different logarithmically equally spaced values of Δt, where the smallest value is the exposure time of the camera.

From the simulation data, we calculate time-resolved autocorrelations of the single-particle potential-energy fluctuations $\Delta u_i(t) = u_i(t) - \langle u_i(t)\rangle_N$, where $\langle \ldots \rangle_N$ indicates the average over all particles $i \in \{1, 2, \ldots, N\}$,

$$C(t, t+\Delta t) = \frac{\langle \Delta u_i(t) \Delta u_i(t+\Delta t)\rangle_N}{\sqrt{\left\langle (\Delta u_i(t))^2 \right\rangle_N \left\langle (\Delta u_i(t+\Delta t))^2 \right\rangle_N}}. \tag{9}$$

Pairwise autocorrelation for time triplets. To verify the triangular relation equation (2), we analysed many time triplets $t_1 < t_2 < t_3$. The analysis focused on the time frame in which $\gamma(t)$ changes, as the triangular relation holds trivially when $\gamma(t) = \text{const}$. In this time frame, 10^3 linearly spaced values of t_1 were chosen. For each t_1, different $t_2 = t_1 + \tau'$ were constructed for 169 logarithmically equally spaced values τ'. Subsequently, for each combination of t_1 and t_2, different $t_3 = t_2 + \tau''$ were constructed using the same 169 logarithmically equally spaced values for τ''. Combined, this procedure generated $1{,}000 \times 169^2 \cong 3 \times 10^7$ different time triplets. For each of these, the pairwise autocorrelations C_{12}, C_{13} and C_{23} (see main text for notation) were calculated using equation (8) with, for example, $t = t_1$ and $t + \tau = t_2$ for the calculation of C_{12}. Finally, subsets with the same values of C_{12} and C_{23} were binned with resolution $\Delta C = 0.005$, and for each subset the mean $\overline{C_{13}}(C_{12}, C_{23})$ and corresponding s.d. $\sigma_{13}(C_{12}, C_{23})$ were calculated.

Constructions of the intensity time series. To obtain the intensity time series in laboratory time $I(t)$, respectively material time $I(\xi)$, intensity fluctuations in one pixel were first interpolated at a tightly spaced sequence of times, where the elapsed time between consecutive points was chosen to be constant either in time or in material time. As the focus is on physical ageing, the analysis is limited to the time frame where $\gamma(t)$ changes (the same time frame as for time triplets). Afterwards, subsets were binned and averaged to obtain a time series of length $N \in \{500, 1{,}000, 2{,}500, 5{,}000, 10{,}000\}$. For $I(\xi)$, this procedure essentially simulates the result we would obtain using a camera operated with a time-dependent exposure time defined by the material-time clock rate. Different N were analysed to ensure that the observed effects are independant of the temporal resolution. As qualitatively equivalent results were obtained for all N, only results for $N = 2{,}500$ are shown in this Article. The above-described procedure was applied to 10^4 different pixels chosen such that the fluctuations are statistically independent. The entire subset was then analysed regarding stationarity and reversibility.

The procedure is very similar for the simulations, except that instead of binning we apply a Gaussian weighted time average at times chosen to be constant either in time or in material time. The width of the Gaussian filter is proportional either to the time clock rate (constant) or the material-time clock rate. This procedure gives very similar results to binning, but is able to filter out very fast fluctuations more efficiently (Supplementary Information). This is necessary for the simulations because of the small dynamic separation between the fast microscopic process and structural relaxation (a consequence of the relatively high temperature at which simulations are performed). As discussed in the Article, the fast process does not age and does not conform to the material-time formalism.

Time-series stationarity analysis. Time-series stationarity is tested by Fourier analysing short sequences of the fluctuations to obtain time-resolved Fourier components. The corresponding procedure involves multiplying the original intensity time series by a Gaussian function for which we can vary the maximum position t_0 to obtain temporal resolution. The obtained 'time-resolved' time series are analysed using the fast Fourier transformation algorithm, and the results are averaged over 10^4 statistically independent time series. More details on the analysis can be found in the Supplementary Information.

Time-series time-reversibility analysis. The time reversibility of $I(t)$ and $I(\xi)$ was analysed using the visibility-graph algorithm[45,46]. This was done by transforming a time series, $I(t)$ respectively $I(\xi)$, and its respective time-inverted time series, $I^r(t)$ respectively $I^r(\xi)$, into a visibility graph using the fast algorithm[76] from the TS2VG python package. Subsequently, the degree distributions were calculated. Finally, the degree distributions of original and time-inverted time series, $P(k)$ and $P^r(k)$, were averaged over 10^4 statistically independent time series. The difference of the two distributions was quantified using the Jensen–Shannon divergence

$$D_{\mathrm{JS}}\left(P(k)||P^r(k)\right) = \frac{1}{2}\left(D_{\mathrm{KL}}(P(k)||\tilde{P}(k)) + D_{\mathrm{KL}}(P^r(k)||\tilde{P}(k))\right), \tag{10}$$

where $\tilde{P}(k) = \frac{1}{2}\left(P(k) + P^r(k)\right)$ and

$$D_{\mathrm{KL}}\left(P(k)||\tilde{P}(k)\right) = \sum_k P(k) \log \frac{P(k)}{\tilde{P}(k)} \tag{11}$$

is the Kullback–Leibler divergence. D_{JS}, which is a symmetric version of D_{KL}, is referred to as the degree of irreversibility in this Article.

Uncertainties for D_{JS} were determined by repeating the above-described analysis ten times for different subsets of 10^4 pixels (no pixel was used in more than one subset). The s.d. of the thus-obtained distributions of D_{JS} are plotted as error bars in Figs. 4 and 5. For the

simulations, the uncertainties of D_{JS} could not be determined due to the limited number of particles.

Due to finite-size effects, $D_{JS} > 0$ even for a time-reversible time series. To obtain the lower limit of D_{JS} that would be approached if the experimentally observed time series were truly time reversible, we performed a surrogate analysis[68]. Numerous surrogate time series of $I(\xi)$ and $I^{-}(\xi)$ were calculated using the iterated amplitude adjusted Fourier transform algorithm[77] and analysed in subsets of 10^4 time series (equivalent to the procedure of analysing experimental time series). The reversibility limits shown in Figs. 4 and 5 correspond to the distribution of D_{JS} obtained by performing several such surrogate analyses.

Data availability

The study generated ~10 TB of data, which are available from the corresponding authors upon request.

Code availability

The code for the analysis of all data sets is available from the corresponding authors upon request.

References

69. Igarashi, B. et al. A cryostat and temperature control system optimized for measuring relaxations of glass-forming liquids. *Rev. Sci. Instrum.* **79**, 045105 (2008).
70. Igarashi, B. et al. An impedance-measurement setup optimized for measuring relaxations of glass-forming liquids. *Rev. Sci. Instrum.* **79**, 045106 (2008).
71. Hecksher, T., Olsen, N. B., Niss, K. & Dyre, J. C. Physical aging of molecular glasses studied by a device allowing for rapid thermal equilibration. *J. Chem. Phys.* **133**, 174514 (2010).
72. Böhmer, T., Gabriel, J. P., Richter, T., Pabst, F. & Blochowicz, T. Influence of molecular architecture on the dynamics of H-bonded supramolecular structures in phenyl-propanols. *J. Phys. Chem. B* **123**, 10959–10966 (2019).
73. Tanaka, H., Meunier, J. & Bonn, D. Nonergodic states of charged colloidal suspensions: repulsive and attractive glasses and gels. *Phys. Rev. E* **69**, 031404 (2004).
74. Bailey, N. P. et al. RUMD: a general purpose molecular dynamics package optimized to utilize GPU hardware down to a few thousand particles. *SciPost Phys.* **3**, 038 (2017).
75. Schrøder, T. B. & Dyre, J. C. Solid-like mean-square displacement in glass-forming liquids. *J. Chem. Phys.* **152**, 141101 (2020).
76. Lan, X., Mo, H., Chen, S., Liu, Q. & Deng, Y. Fast transformation from time series to visibility graphs. *Chaos* **25**, 083105 (2015).
77. Schreiber, T. & Schmitz, A. Improved surrogate data for nonlinearity tests. *Phys. Rev. Lett.* **77**, 635–638 (1996).

Acknowledgements

We thank M. Zanin and S. Ditlevsen for advice regarding the data analysis. This work was supported by the VILLUM Foundation's Matter grant (VIL16515) and by the Deutsche Forschungsgemeinschaft (grants BL 923/1 and BL 1192/3).

Author contributions

J.C.D. and T. Blochowicz devised the project; T. Böhmer and J.P.G. planned the experiments; T. Böhmer, J.P.G. and J.-N.K. performed the experiments; T. Böhmer and J.P.G. analysed the experimental data; L.C. and T. Böhmer performed and analysed the computer simulations; T.H., J.C.D. and T. Blochowicz supervised the experiments and data analysis, T. Böhmer and J.C.D. wrote the paper with input from all authors; J.C.D. and T. Blochowicz provided resources and acquired funding.

Competing interests

The authors declare no competing interests.

Additional information

Supplementary information The online version contains supplementary material available at https://doi.org/10.1038/s41567-023-02366-z.

Correspondence and requests for materials should be addressed to Till Böhmer, Jeppe C. Dyre or Thomas Blochowicz.

Peer review information *Nature Physics* thanks Isabella Gallino, Yoav Lahini, and the other, anonymous, reviewer(s) for their contribution to the peer review of this work.